Journal of Alloys and Compounds 509S (2011) S567–S571

Contents lists available at ScienceDirect

Journal of Alloys and Compounds

journal homepage: www.elsevier.com/locate/jallcom

Layer-resolved study of the Mg to MgH_2 transformation in Mg–Ti films with short-range chemical order

S.W.H. Eijt[a,*], H. Leegwater[a], H. Schut[a], A. Anastasopol[a], W. Egger[b], L. Ravelli[b], C. Hugenschmidt[c], B. Dam[d]

[a] Department of Radiation, Radionuclides and Reactors, Faculty of Applied Sciences, Delft University of Technology, Delft, The Netherlands
[b] Institut für Angewandte Physik und Messtechnik, Universität der Bundeswehr München, Neubiberg, Germany
[c] ZWE FRM II, Technische Universität München, Garching, Germany
[d] Department of Chemical Engineering, Faculty of Applied Sciences, Delft University of Technology, Delft, The Netherlands

ARTICLE INFO

Article history:
Received 30 June 2010
Received in revised form
23 September 2010
Accepted 26 September 2010
Available online 2 October 2010

Keywords:
Hydrogen storage materials
Thin films
Vapour deposition
Positron annihilation
Vacancies
Metal–insulator transition

ABSTRACT

Positron depth-profiling was applied to monitor the effects of hydrogenation on $Mg_{1-y}Ti_y$ thin films. *S–W* diagrams and VEPFIT analysis of the depth-profiles demonstrated the homogeneity of most metal and metal hydride films. In contrast, $Mg_{0.90}Ti_{0.10}H_x$ films consisted of a double layer, with a thin unloaded $Mg_{0.90}Ti_{0.10}$ or Mg–Ti–Pd alloy layer on top of a hydrogenated bottom layer. The metal-to-metal-hydride transformation of Mg domains in the nanoscale phase-segregated Mg–Ti films was monitored exclusively, enabled by the large difference in positron affinity for Mg and Ti. The changes in the Doppler broadening parameters revealed that the metal–insulator transition for fluorite MgH_2 is similar to that for rutile MgH_2. Positron lifetime spectroscopy showed the presence of di-vacancies in the metal sub-lattice of as-deposited and hydrogenated Mg–Ti metal films, which may induce the fast hydrogen sorption kinetics of the fluorite MgH_2 phase.

1. Introduction

Mg-based metals are promising materials for application as hydrogen storage media [1], metal hydride rechargeable batteries [2] and hydrogen sensors [3]. Mg–Ti alloys are of interest in order to overcome the bottleneck of slow hydrogen sorption kinetics of rutile MgH_2 at practical temperatures for applications. Important feature is the appearance of a meta-stable fluorite $Mg_{1-y}Ti_yH_x$ phase upon hydrogenation of films with Ti-concentrations larger than ~15% ($Mg_{0.85}Ti_{0.15}$), showing substantially faster hydrogenation kinetics than the rutile phase [4].

In order to clarify the dependence of hydrogenation of Mg–Ti films on Ti-concentration, it is therefore important to shed light on the (layer-resolved) metal hydride formation. Motivated by previous studies on Mg-based metal films [5,6], we apply positron depth-profiling. While X-ray diffraction studies indicate that co-deposition of Mg and Ti by magnetron sputtering leads to Mg–Ti films with a coherent crystal structure, positron annihilation and EXAFS studies strongly indicate that atomically mixed alloys are not formed. Instead, partial chemical segregation occurs into Mg and Ti domains on a length scale of less than 10 nm [7,8].

Here, we show that positron annihilation and X-ray diffraction studies reveal highly complementary information, needed to unravel the layer-dependent phase transformations. Furthermore, a direct view on the metal–insulator transition of the nanoscale segregated Mg areas in the Mg–Ti films is obtained by the positron Doppler broadening method, owing to its sensitivity to detect the electronic structure via the electron momentum distribution (EMD). This is important in order to understand the remarkable but also complex optical changes during hydrogenation of Mg–Ti films [9], which show promise as switchable smart solar collectors [9]. Finally, depth-profiling positron annihilation lifetime spectroscopy (PALS) provided clear evidence for the presence of di-vacancies in the metal sub-lattice of the metal hydride and metal films, which may have important impact on the hydrogen mobility.

2. Experimental details

Mg–Ti films were deposited in a UHV system by RF magnetron co-sputtering of Mg and Ti targets in argon atmosphere, on suprasil glass substrates, and covered with a 1–5 nm Pd capping layer. Four $Mg_{0.90}Ti_{0.10}$, four $Mg_{0.70}Ti_{0.30}$ and two Ti film samples were pre-

* Corresponding author. Tel.: +31 15 278 9053; fax: +31 15 278 6422.
E-mail address: s.w.h.eijt@tudelft.nl (S.W.H. Eijt).

0925-8388/$ – see front matter © 2010 Elsevier B.V. All rights reserved.
doi:10.1016/j.jallcom.2010.09.157

pared with layer thicknesses in the range 150–250 nm. Two of the $Mg_{0.90}Ti_{0.10}$ samples were hydrogenated for a period of 24 h using pressures slowly increasing up to 90 mbar at room temperature. The hydrogenation of two $Mg_{0.70}Ti_{0.30}$ and two Ti samples was performed at 100 and 500 mbar, respectively, for 1 h at room temperature.

X-ray diffraction (XRD) was performed using a Panalytical X'Pert Pro PMD X-ray Diffractometer (Cu Kα, λ = 1.54187 Å), and X-ray reflectometry (XRR) using a Panalytical X'Pert Pro MRD reflectometer.

The positron Doppler broadening of annihilation radiation (511 keV) was measured using positrons with a kinetic energy in the range of 0–25 keV. Momentum windows $|p| < 3.0 \times 10^{-3} m_o c$ and $8.2 \times 10^{-3} m_o c < |p| < 23.4 \times 10^{-3} m_o c$ for *S* and *W*, respectively, were used [10] (see inset of Fig. 1b). The *S* parameter is a measure of annihilation with valence electrons, providing sensitivity to the electronic structure and the presence of vacancies, while *W* is a measure for positron annihilation with semi-core electrons, providing chemical sensitivity to the positron trapping site. The *S* and *W* parameter depth-profiles were analyzed using the VEPFIT program package [11]. Consistent fits of the *S* and *W* depth profiles could be achieved using a combined analysis with the same layered model parameters.

Thin film positron annihilation lifetime spectroscopy (PALS) was performed using the pulsed low energy positron beam system (PLEPS) [12]. The positron lifetime is a direct measure of the local electron density at the positron annihilation site, which can be used to extract the size of vacancy-related defects [13]. Positron lifetime spectra were collected at selected positron implantation energies in the range of 0.5–18 keV. Typically 4×10^6 counts were collected for each individual lifetime spectrum. Reference spectra at each implantation energy were collected on a p-SiC reference sample to extract the overall instrumental time resolution function with a FWHM of 260 ps, which includes the time resolution of the detector and the pulse width of the incident positron beam. The spectra were fitted using the POSWIN software package [14] using a three-lifetime component analysis.

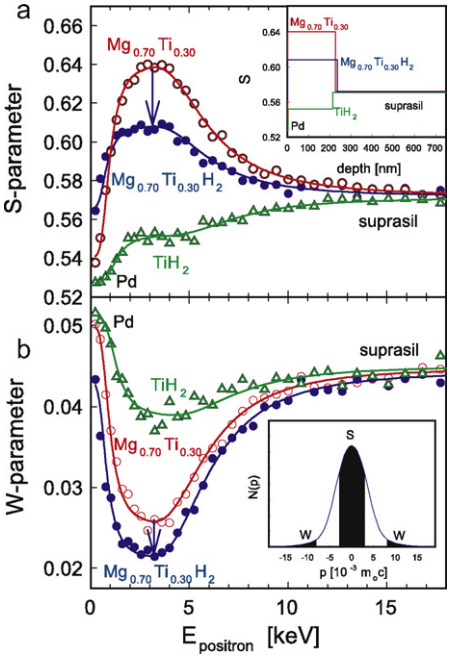

Fig. 1. (a) Doppler *S*-parameter depth profiles for as-deposited (hollow circles) and hydrogenated (filled circles) Pd-capped $Mg_{0.70}Ti_{0.30}$ films, compared with a Pd-capped TiH_2 layer (hollow triangles). The solid lines are fits obtained using VEPFIT. The inset shows the layered structure of the samples deduced from the VEPFIT analysis. (b) Corresponding Doppler *W*-parameter depth-profiles. The shaded areas in the inset denote the intervals used to determine the *S*- and *W*-parameters from the measured electron-positron momentum distribution *N*(*p*).

3. Results and discussion

3.1. Doppler depth profiling of metal hydride thin films

In order to extract the layer-resolved phase transformation of Mg–Ti films, we performed positron Doppler broadening studies on as-deposited and hydrogen loaded $Mg_{0.70}Ti_{0.30}$ films. Fig. 1 shows representative *S* and *W* depth-profiles in a comparison with one of the TiH_2 films. Upon hydrogenation, the S-parameter of the $Mg_{0.70}Ti_{0.30}$ layer reduces significantly in the range of 1–5 keV in positron implantation energy, for which a substantial fraction of positrons annihilates in the metal (hydride) layer. The change in S-parameter is similar in magnitude as for the Mg to MgH_2 transformation in Mg [5–7] and $Mg_{0.90}Ti_{0.10}$ films [7]. Our previous studies [5,15] demonstrated that such a large reduction in S-parameter is a direct result of the metal–insulator transition upon hydrogenation to the MgH_2 phase. Mg metal, namely, has a free-electron-like electronic structure with a Fermi momentum cut-off at $p_F \sim 5.3 \times 10^{-3} m_o c$ [5], leading to a relatively sharp valence electron momentum distribution (EMD) [5]. Rutile phase MgH_2, on the other hand, is an insulator with primarily ionic Mg–H bonds with more localized valence electron orbitals. This leads to a substantial broadening of the electron momentum distribution upon transition to the insulator phase, resulting in the observed strong reduction in *S*-parameter [15].

The *S* and *W* depth profiles were analyzed using VEPFIT, which solves the implantation–diffusion equation for positrons implanted at selected energies assuming a layered model of the sample, and fits calculated *S* and *W* curves to the experimental depth-profiles [11] (Fig. 1). The $Mg_{0.70}Ti_{0.30}$ and $Mg_{0.70}Ti_{0.30}H_2$ films each clearly consists of a single homogeneous layer, capped by a ~1 nm thin Pd layer. The TiH_2 film was capped by a somewhat thicker Pd layer of ~4 nm. The inset of Fig. 1a shows the layered structure of the films extracted from the VEPFIT analysis.

In Fig. 2 we present the corresponding *S*–*W* diagram for a set of $Mg_{1-y}Ti_y$ metal and metal hydride films. The experimental data and VEPFIT curves for the $Mg_{0.70}Ti_{0.30}$, $Mg_{0.70}Ti_{0.30}H_2$ and $Mg_{0.90}Ti_{0.10}$ films are characterized by straight lines in the *S*–*W* diagram, reflecting the single layer behavior of the metal (hydride) layer. The *S*–*W* data for the hydrogenated $Mg_{0.90}Ti_{0.10}H_x$ film, in contrast, shows a loop behavior. This proofs that the latter film actually consists of a double-layer. The loop in the *S*–*W* curve shows that, with increasing

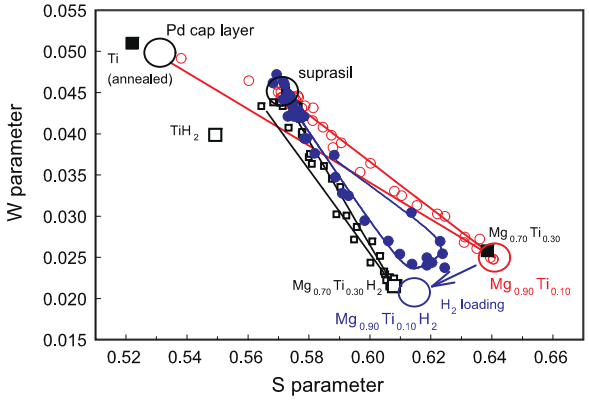

Fig. 2. *S*–*W* diagram for as-deposited $Mg_{0.90}Ti_{0.10}$ (hollow circles) and hydrogenated $Mg_{0.70}Ti_{0.30}H_2$ (hollow squares) and $Mg_{0.90}Ti_{0.10}H_x$ (filled circles) films; the running parameter is the positron implantation energy *E*. The solid lines are extracted from the combined VEPFIT analysis of the *S* and *W* depth profiles.

positron implantation energy, the positrons first detect the Pd cap layer, and subsequently annihilate primarily in an upper unloaded $Mg_{0.90}Ti_{0.10}$ metal layer, with *S* and *W* values close to those of Mg. At higher energies, the *S*–*W* curve turns towards lower *S* and *W* values characteristic for the $Mg_{0.90}Ti_{0.10}H_2$ metal hydride phase in the bottom layer, before it takes a second turn towards the *S*–*W* point of the suprasil substrate at the highest implantation energies. Clearly, the *S*–*W* curve extracted from VEPFIT assuming a double layer structure for the $Mg_{0.90}Ti_{0.10}H_x$ film fits the experimental data in an excellent manner.

3.2. Crystal phase identification from X-ray diffraction

X-ray diffraction provided further insight into the double-layered nature of the $Mg_{0.90}Ti_{0.10}H_x$ film. Fig. 3 shows that one distinct intense Mg–Ti (0 0 2) peak is observed for the $Mg_{0.90}Ti_{0.10}$ and $Mg_{0.70}Ti_{0.30}$ samples. The diffraction peak positions are close to that of hcp-Mg, showing a small *c*-axis lattice contraction due to the incorporated Ti [8,16]. The diffraction pattern for the hydrogenated $Mg_{0.90}Ti_{0.10}H_x$ film, in contrast, revealed the presence of two diffraction peaks corresponding to two different phases present in the film, one coinciding with hexagonal $Mg_{0.90}Ti_{0.10}$ present in the metal top layer and a second, broad peak related to the rutile phase $Mg_{0.90}Ti_{0.10}H_2$ bottom layer. In contrast, the position of the single broad diffraction peak for the hydrogenated $Mg_{0.70}Ti_{0.30}H_2$ sample is typical for the fluorite metal hydride phase which stabilizes for Ti-fractions larger than about 15 at% [16,8], including the TiH_2 phase (bottom of Fig. 3).

3.3. Double layer behavior of $Mg_{90}Ti_{10}H_x$ films

Fig. 4 shows the experimental depth-profiles of as-deposited and hydrogenated $Mg_{0.90}Ti_{0.10}$ films and the corresponding VEPFIT modeling curves. The double-layer model for the $Mg_{0.90}Ti_{0.10}H_x$ film leads to a satisfactory fit, showing the presence of a thin unloaded metal layer on top of a thick metal hydride layer, consistent with the XRD detection of both phases. The relatively weak intensity and broadness of the rutile phase $Mg_{0.90}Ti_{0.10}H_2$ (1 1 0) diffraction peak stems from (small-angle) tilting of metal hydride domains relative to the sample surface [17,5]. In contrast, the c-axis of the hexagonal $Mg_{0.90}Ti_{0.10}$ phase is well-aligned [17,5], leading to the relatively large intensity of the $Mg_{0.90}Ti_{0.10}$ (0 0 2) peak. We believe that the double layer formation may arise from either the more difficult hydrogenation of Mg–Ti films with Ti-compositions below ~15%, for which rutile phase MgH_2 stabilizes, or, perhaps, partial desorption due to air contact. The presence of the metal top layer thus seems to indicate that the hydride forms from the substrate side, as described in [18]. An alternative explanation for the top layer could be the formation of a Mg-rich Mg–Ti–Pd alloy layer with a thickness of ~20 nm, a possibility consistent with the initial presence of the 1–2 nm Pd cap layer and the *S*–*W* values detected near the surface.

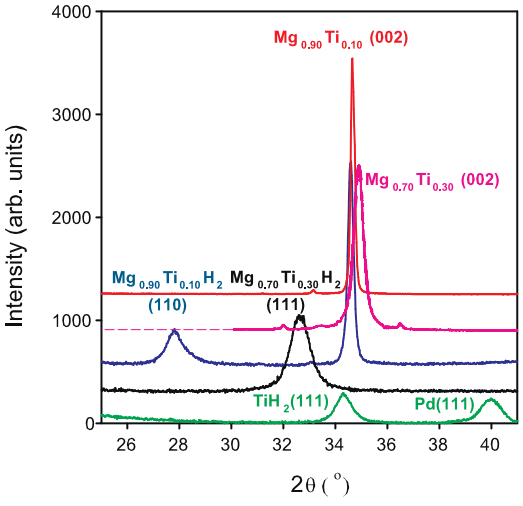

Fig. 3. X-ray diffraction patterns for as-deposited $Mg_{0.90}Ti_{0.10}$ and $Mg_{0.70}Ti_{0.30}$ films compared with hydrogenated $Mg_{0.90}Ti_{0.10}H_x$, $Mg_{0.70}Ti_{0.30}H_2$ and TiH_2 films (top to bottom).

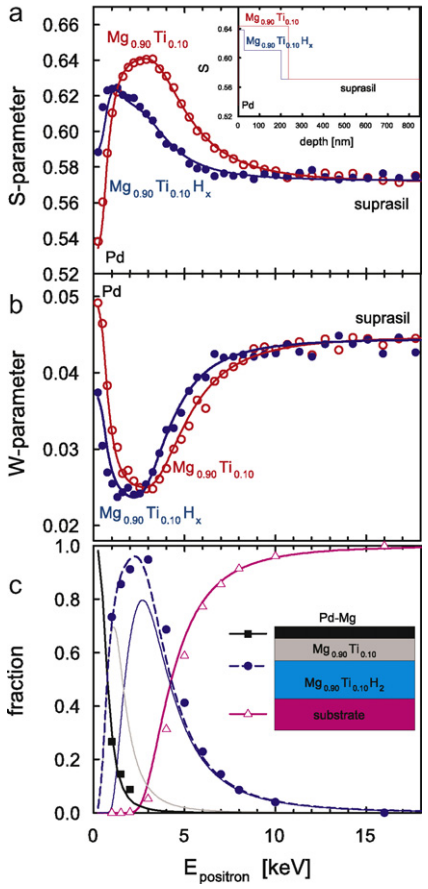

Fig. 4. (a) *S*-parameter depth profiles for as-deposited (hollow circles) and hydrogenated (filled circles) Pd-capped $Mg_{0.90}Ti_{0.10}$ films. The solid lines are fits obtained using VEPFIT. The inset shows the layered structure of the samples deduced from VEPFIT analysis of the *S* and *W* depth profiles. (b) Corresponding *W*-parameter depth-profiles. (c) Fractions of positrons annihilating in the Pd cap layer (solid squares), in the $Mg_{0.90}Ti_{0.10}$ metal and $Mg_{0.90}Ti_{0.10}H_2$ metal hydride layers (filled circles), and in the suprasil substrate (open triangles) as a function of positron implantation energy, derived from the PALS study (symbols) and VEPFIT analysis of the Doppler *S*–*W* depth-profiles (lines).

Interestingly, the *S*–*W* cluster points for the $Mg_{0.70}Ti_{0.30}$ and $Mg_{0.90}Ti_{0.10}$ layers in the *S*–*W* diagram (Fig. 2) show similar clear and large shifts upon hydrogenation, typical for the Mg to MgH_2 metal-to-insulator transition [5,15]. In Refs. [7,8] it was shown that the Mg–Ti films consist of Mg regions which are chemically segregated from Ti domains. The positron detects the presence of Mg domains only, because of the large difference in positron affinity for Mg metal compared with Ti [7], leading to trapping in the Mg regions before annihilation. This enabled us to monitor the metal-to-insulator transition in the Mg regions of the $Mg_{1-y}Ti_y$ films exclusively. Consistency with XRD requires that the segregation into Mg and Ti domains takes place on a length scale below the coherence length of X-ray scattering, i.e. well below ~10 nm. A particularly interesting finding is the close similarity of the change in Doppler broadening parameters for $Mg_{0.70}Ti_{0.30}$ and $Mg_{0.90}Ti_{0.10}$

Table 1
Layer thicknesses derived from positron depth-profiling (DBAR) and X-ray reflectometry (XRR).

Compound	Thickness (nm) DBAR	Thickness (nm) XRR
$Mg_{0.90}Ti_{0.10}H_x$ (second sample)	175 ± 18	189 ± 5
TiH_2	196 ± 20	163 ± 5

upon hydrogenation. This provides a strong indication that the metal-to-insulator transition for rutile and fluorite phase MgH_2 is similar.

In order to quantify the Doppler depth profiling results further, we compare the deduced thicknesses of the layers with X-ray reflectometry measurements (Table 1), which points at similar thicknesses. Note that in the XRR study the contrast between the unloaded metallic $Mg_{0.90}Ti_{0.10}$ top layer and the hydrogenated $Mg_{0.90}Ti_{0.10}H_2$ bottom layer was too small to resolve the presence of two individual layers, owing to their similar densities of 2.0 and 1.6 g/cm^3, respectively. For the TiH_2 layer, a density of 3.75 g/cm^3 was used in the VEPFIT analysis.

3.4. Positron lifetime study on vacancy-related defects

We further compared the implantation-energy-dependent annihilation fractions of positrons annihilating in either of the layers, as obtained from the VEPFIT analysis, with the fractions extracted from the PALS study (Fig. 4c). Clearly, the fractions extracted by the two methods are in a quantitative agreement. The extraction of the fractions from the PALS study was enabled by the quite distinct positron lifetimes of the main lifetime component in the Pd top layer (~200 ps), the Mg–Ti layers (~300 ps) and the suprasil substrate (with a long lifetime component of ~1.6 ns). The fractions were derived via variation of the relative intensities using POSWIN. The spectra were generally analyzed in a three-lifetime component fit. Except for the lowest implantation energies, the third lifetime component corresponded to a long lifetime of ~1.6 ns, which gained significant intensity for implantation energies beyond about 3 keV when positrons start to detect the substrate. The 1.6 ns lifetime component is typical for small voids with sizes below ~1 nm, which are present only in the suprasil substrate, and is easily discriminated from the other, shorter lifetime components. The positron lifetime spectrum in the Pd top layer is dominated by a short lifetime component of about 200 ps, whereas the spectrum for the Mg–Ti(–H) layer is characterized by a ~300 ps lifetime component, respectively. The annihilation fraction in the top Pd layer can therefore also be extracted straightforwardly (Fig. 4c). The difference in positron lifetimes between $Mg_{0.90}Ti_{0.10}$ and $Mg_{0.90}Ti_{0.10}H_2$ (Table 2) was too small to obtain their separate intensities as a function of energy reliably. Therefore, the extracted summed fraction of annihilation in the top metal and bottom metal hydride layer is used in Fig. 4c.

In Ref. [7], we showed that the extracted positron lifetime of 312 ± 4 ps for the Mg film indicates that the positron trapping defect is the di-vacancy. The observed saturation trapping also accounted for the very short positron diffusion lengths of less than 5 nm for all $Mg_{1-y}Ti_y$ and $Mg_{1-y}Ti_yH_x$ layers, as deduced by the VEPFIT analysis.

Table 2
Positron lifetimes of $Mg_{1-y}Ti_y$ and $Mg_{1-y}Ti_yH_2$ layers.

Compound	Positron lifetime (ps)
Mg	312 ± 4
$Mg_{0.90}Ti_{0.10}$	297 ± 4
$Mg_{0.70}Ti_{0.30}$	275 ± 4
$Mg_{0.90}Ti_{0.10}H_2$	317 ± 6
$Mg_{0.70}Ti_{0.30}H_2$	312 ± 4
TiH_2	185 ± 9

The increasingly smaller positron lifetime with increased Ti fraction for the $Mg_{1-y}Ti_y$ metals (Table 2) arises from the corresponding contraction in unit cell volume. Clearly, the positron lifetime for the TiH_2 layer is far lower than for the $Mg_{1-y}Ti_yH_x$ films, providing further evidence that MgH_2 regions are probed in the metal hydride films. Our previous study [7] indicated that di-vacancies are present in the metal sub-lattice of both the rutile and fluorite MgH_2 phases. While the lifetimes of these vacancies are similar (Table 2), pointing to a similar size of the di-vacancy in the rutile and the fluorite phase, the sizes of their unit cells differ considerably. Therefore, we deduce the existence of local lattice relaxations around the di-vacancy in the fluorite phase, which may play a crucial role in the enhanced hydrogen transport in fluorite MgH_2 [7].

4. Conclusions

Positron depth-profiling methods were applied to examine the metal-to-metal-hydride transformation in Mg–Ti thin films. Combined *S*–*W* analysis leads to reliable extraction of the layer-resolved composition of the films. While single homogeneous layers are commonly observed, $Mg_{0.90}Ti_{0.10}H_x$ films show the presence of a double layer, with a desorbed or unloaded Mg–Ti(–Pd) metal layer on top of the metal hydride layer. Positrons probe the chemically segregated Mg regions in the Mg–Ti films exclusively, and demonstrate the similarity in the metal–insulator transition to either the rutile or fluorite MgH_2 phase. The information gained is highly complementary to that from X-ray diffraction and reflectometry, as it provides insights into the layered structure of the metal and metal hydride films, the nanoscale chemical segregation in Mg–Ti films and the presence of vacancies which may play an important role in the hydrogen mobility.

Acknowledgments

We thank Herman Schreuders for preparation of the samples. Ruud Hendrikx at the Department of Materials Science and Engineering of Delft University of Technology is acknowledged for the X-Ray Reflectometry (XRR) analysis. This work benefited from financial support by Senter Novem through the EOS grant LT07052. The project was supported by the European Commission under the 7th Framework Programme, Key Action: Strengthening the European Research Area, Research Infrastructures. Contract No.: 226507 (NMI3). The work at the Department of Chemical Engineering was supported by the Nederlandse Organisatie voor Wetenschappelijk Onderzoek (NWO) through the Sustainable Hydrogen Programme of ACTS.

References

[1] L. Schlapbach, A. Züttel, Nature 414 (2001) 353–358.
[2] R.A.H. Niessen, P.H.L. Notten, Electrochem. Solid-State Lett. 8 (2005) A534–538.
[3] M. Slaman, B. Dam, H. Schreuders, R. Griessen, Int. J. Hydrogen Energy 33 (2008) 1084–1089.
[4] P. Vermeulen, R.A.H. Niessen, D.M. Borsa, B. Dam, R. Griessen, P.H.L. Notten, Electrochem. Solid-State Lett. 9 (2006) A520–A523.
[5] S.W.H. Eijt, R. Kind, S. Singh, H. Schut, W.J. Legerstee, R.W.A. Hendrikx, V.L. Svetchnikov, R.J. Westerwaal, B. Dam, J. Appl. Phys. 105 (2009) 043514.
[6] R. Checchetto, N. Bazzanella, A. Miotello, R.S. Brusa, A. Zecca, A. Mengucci, J. Appl. Phys. 95 (2004) 1989–1995.
[7] H. Leegwater, H. Schut, W. Egger, A. Baldi, B. Dam, S.W.H. Eijt, Appl. Phys. Lett. 96 (2010) 121902.
[8] A. Baldi, R. Gremaud, D.M. Borsa, C.P. Baldé, A.M.J. van der Eerden, G.L. Kruijtzer, P.E. de Jongh, B. Dam, R. Griessen, Int. J. Hydrogen Energy 34 (2009) 1450–1457.
[9] D.M. Borsa, A. Baldi, M. Pasturel, H. Schreuders, B. Dam, R. Griessen, P. Vermeulen, P.H.L. Notten, Appl. Phys. Lett. 88 (2006) 241910.
[10] A. van Veen, H. Schut, P.E. Mijnarends, in: P.G. Coleman (Ed.), Positron Beams and their Applications, World Scientific, Singapore, 2000 (Chapter 6).
[11] A. van Veen, H. Schut, J. de Vries, R.A. Hakvoort, M.R. IJpma, AIP Conf. Proc. Vol. 218 (1990) 171–196.

[12] W. Egger, P. Sperr, G. Kögel, G. Dollinger, Phys. Stat. Solidi (c) 4 (2007) 3969–3972.
[13] R. Krause-Rehberg, H.S. Leipner, Positron Annihilation in Semiconductors: Defect Studies, Springer Verlag, Berlin, 1999.
[14] D. Bochert, Diploma Thesis, Universität der Bundeswehr München, 2004.
[15] S.W.H. Eijt, Phys. Stat. Solidi (c) 6 (2009) 2561–2565.
[16] P. Vermeulen, P.C.J. Graat, H.J. Wondergem, P.H.L. Notten, Int. J. Hydrogen Energy 33 (2008) 5646–5650.
[17] R. Kelekar, H. Giffard, S.T. Kelly, B.M. Clemens, J. Appl. Phys. 101 (2007) 114311.
[18] W. Lohstroh, R.J. Westerwaal, B. Noheda, S. Enache, I.A.M.E. Giebels, B. Dam, R. Griessen, Phys. Rev. Lett. 93 (2004) 197404.